Comptes Rendus

Mécanique

Carlos N. Tomé and Ricardo A. Lebensohn

Polycrystal thermo-elasticity revisited: theory and applications

Contributions in mechanics of materials

Polycrystal thermo-elasticity revisited: theory and applications

Carlos N. Tomé[a] and Ricardo A. Lebensohn[*, a]

[a] Los Alamos National Laboratory, Los Alamos, NM 87544, USA

E-mails: tome@lanl.gov (C. N. Tomé), lebenso@lanl.gov (R. A. Lebensohn)

Abstract. The self-consistent (SC) theory is the most commonly used mean-field homogenization method to estimate the mechanical response behavior of polycrystals based on the knowledge of the properties and orientation distribution of constituent single-crystal grains. The original elastic SC method can be extended to thermo-elasticity by adding a stress-free strain to an elastic constitutive relation that expresses stress as a linear function of strain. With the addition of this independent term, the problem remains linear. Although the thermo-elastic self-consistent (TESC) model has important theoretical implications for the development of self-consistent homogenization of non-linear polycrystals, in this paper, we focus on TESC applications to actual thermo-elastic problems involving non-cubic (i.e. thermally anisotropic) materials. To achieve this aim, we provide a thorough description of the TESC theory, which is followed by illustrative examples involving cooling of polycrystalline non-cubic metals. The TESC model allows studying the effect of crystallographic texture and single-crystal elastic and thermal anisotropy on the effective thermo-elastic response of the aggregate and on the internal stresses that develop at the local level.

Keywords. Homogenization, Self-consistent methods, Thermo-elasticity, Polycrystals, Anisotropy, Metals.

Manuscript received 7th May 2020, revised and accepted 6th July 2020.

1. Introduction

The self-consistent (SC) theory is the most commonly used mean-field homogenization method for estimating the mechanical response behavior of polycrystals based on the knowledge of the properties and orientation distribution of constituent single-crystal grains. The SC method was proposed independently by Hershey [1] and Kröner [2] for linear elastic polycrystals, and it was subsequently expanded for this constitutive regime by Hill [3] and Zeller and Dederichs [4]. Although in the early days of the formulation, computational restrictions limited the applications of SC models to relatively simple cases, a general implementation of the elastic SC model is now part of homogenization-based polycrystal mechanics codes such as the VPSC code [5].

Consideration of thermo-elasticity adds a stress-free strain to the elastic constitutive relation that expresses stress as a linear function of strain. With the addition of this independent term,

---

* Corresponding author.

the problem remains linear. The solution of a thermo-elastic self-consistent (TESC) problem for composites, consisting of a phase made of inclusions embedded in a matrix phase with different mechanical properties, was introduced by Walpole [6] and further reformulated and extended by, for example, Willis [7], Buryachenko [8], and Milton [9]. These works identified and, in some cases, also tackled the case of polycrystals as a special composite made of many *mechanical* phases, with distinct properties associated with different single-crystal orientations, with no matrix phase. Tomé *et al.* [10] presented the TESC formulation specialized for polycrystals to predict the thermo-mechanical response of hexagonal close packed (hcp) Zr aggregates, which, as almost every non-cubic material, has anisotropic thermal properties at the single-crystal level. The TESC formulation also has important theoretical implications for the development of SC homogenization of non-linear polycrystals. Indeed, for aggregates of grains deforming in the viscoplastic regime, the different available SC theories vary in the procedure used to linearize the non-linear mechanical behavior at the grain level, but eventually all of them make use of the TESC theory applied to the linearized behavior of an iteratively adjusted generalized thermo-elastic polycrystalline material.

Despite its relevance, a thorough exposition of the TESC theory with applications to actual thermo-elastic polycrystal problems is lacking in the literature. Only a brief description can be found in [10] as one among several applications of different SC models to different deformation regimes (TESC being one of them) for the interpretation of experimental data on Zr alloys. The present contribution intends to fill this gap by presenting the polycrystal TESC theory in a comprehensive manner, which is followed by illustrative examples involving cooling of polycrystalline non-cubic metals to study the effect of crystallographic texture and single-crystal elastic and thermal anisotropy on the effective and local thermo-elastic responses of the aggregate.

2. Model

In the context of the SC theory, a polycrystal is represented by a set of weighted crystal orientations. The orientations represent mechanical phases (i.e. set of single-crystal grains with the same orientation and morphology surrounded by different neighborhoods) or statistically representative "grains" (in what follows, "grains" and mechanical phases will be used interchangeably), and the weights represent volume fractions. The set of orientations and weights is chosen to reproduce the initial crystallographic texture of the material. Each grain is treated as an *ellipsoidal elastic inhomogeneous inclusion* embedded in an *effective homogenized thermo-elastic medium*. The ellipsoidal shape (or distribution of ellipsoidal shapes) represents the morphologic texture of the polycrystal. The inhomogeneity character derives from the difference in elastic properties between each individual grain and the effective homogenized medium when expressed in the same reference system. The inclusion character derives from the possible presence of eigenstrains such as thermal strains. The inhomogeneous inclusions and the medium generally have fully anisotropic properties, deriving from the intrinsic single-crystal anisotropy, crystallographic texture, and/or non-equiaxed morphology. The effective medium represents the average environment surrounding each orientation. Deformation is based on anisotropic crystal elasticity and thermal expansion, which in the case of non-cubic crystals is also anisotropic.

2.1. *Local constitutive behavior and homogenization*

The local thermo-elastic constitutive behavior in a material point **x** of the polycrystal, relating the local strain $\boldsymbol{\varepsilon}(\mathbf{x})$ and stress $\boldsymbol{\sigma}(\mathbf{x})$ is described by the linear relation

$$\varepsilon_{ij}(\mathbf{x}) = C_{ijkl}^{-1}(\mathbf{x})\sigma_{kl}(\mathbf{x}) + \alpha_{ij}(\mathbf{x})\delta T(\mathbf{x}) = \varepsilon_{ij}^{\text{el}}(\mathbf{x}) + \varepsilon_{ij}^{\text{th}}(\mathbf{x}), \tag{1}$$

$$\sigma_{ij}(\mathbf{x}) = C_{ijkl}(\mathbf{x})(\varepsilon_{kl}(\mathbf{x}) - \varepsilon_{kl}^{\text{th}}(\mathbf{x})), \tag{2}$$

where the moduli $\mathbf{C}(\mathbf{x})$ and $\boldsymbol{\alpha}(\mathbf{x})$ are the elastic stiffness and the thermal expansion tensors of the single crystal containing the material point $\mathbf{x}$, which, in general, can be considered to be piecewise constant within the domain of each grain (g) and thus can be denoted by $\mathbf{C}^{(g)}$ and $\boldsymbol{\alpha}^{(g)}$, respectively; $\delta T(\mathbf{x})$ is the change in local temperature from the temperature at which the aggregate is free of thermal stresses; and $\boldsymbol{\varepsilon}^{\text{el}}(\mathbf{x})$ and $\boldsymbol{\varepsilon}^{\text{th}}(\mathbf{x})$ are the elastic and thermal strains, respectively. The thermal strain can be regarded as a stress-independent eigenstrain induced by temperature change.

Assuming uniform temperature distribution, the following relation holds within the domain of grain (g):

$$\boldsymbol{\sigma}(\mathbf{x}) = \mathbf{C}^{(g)} : \boldsymbol{\varepsilon}(\mathbf{x}) - \mathbf{C}^{(g)} : \boldsymbol{\alpha}^{(g)} \delta T, \tag{3}$$

$$\boldsymbol{\varepsilon}(\mathbf{x}) = \mathbf{C}^{(g)^{-1}} : \boldsymbol{\sigma}(\mathbf{x}) + \boldsymbol{\alpha}^{(g)} \delta T, \tag{4}$$

where δT is the uniform change in temperature from the temperature at which the aggregate is free of thermal stresses. At the aggregate level, a similar constitutive law holds, involving the effective elastic and thermal moduli:

$$\overline{\boldsymbol{\sigma}} = \overline{\mathbf{C}} : \overline{\boldsymbol{\varepsilon}} - \overline{\mathbf{C}} : \overline{\boldsymbol{\alpha}} \delta T, \tag{5}$$

$$\overline{\boldsymbol{\varepsilon}} = \overline{\mathbf{C}}^{-1} : \overline{\boldsymbol{\sigma}} + \overline{\boldsymbol{\alpha}} \delta T. \tag{6}$$

The bars on top indicate the polycrystal's effective tensors. The effective elastic stiffness $\overline{\mathbf{C}}$ and effective thermal expansion $\overline{\boldsymbol{\alpha}}$ are *a priori* unknown and need to be determined. From Hill's lemma [11], the volume averages of the local stress and strain tensors, denoted here as $\langle \ \rangle$, correspond to the effective magnitudes $\overline{\boldsymbol{\varepsilon}} = \langle \boldsymbol{\varepsilon}(\mathbf{x}) \rangle$ and $\overline{\boldsymbol{\sigma}} = \langle \boldsymbol{\sigma}(\mathbf{x}) \rangle$, respectively. Taking volumetric average of (3) and (4), and using (5) and (6), respectively, leads to the following relations:

$$\overline{\mathbf{C}} : \overline{\boldsymbol{\varepsilon}} - \overline{\mathbf{C}} : \overline{\boldsymbol{\alpha}} \delta T = \langle \mathbf{C}^{(g)} : \boldsymbol{\varepsilon}(\mathbf{x}) \rangle - \langle \mathbf{C}^{(g)} : \boldsymbol{\alpha}^{(g)} \rangle \delta T, \tag{7}$$

$$\overline{\mathbf{C}}^{-1} : \overline{\boldsymbol{\sigma}} + \overline{\boldsymbol{\alpha}} \delta T = \langle \mathbf{C}^{(g)^{-1}} : \boldsymbol{\sigma}(\mathbf{x}) \rangle + \langle \boldsymbol{\alpha}^{(g)} \rangle \delta T. \tag{8}$$

These relations couple the elastic and thermal tensors of the grain with those of the aggregate, and they are completely general. In this work, we provide the algorithm to solve for $\overline{\mathbf{C}}$ and $\overline{\boldsymbol{\alpha}}$ within the framework of the TESC formulation. However, before describing the latter, it is instructive to present the also commonly used upper-bound (UB) and lower-bound (LB) approaches. The simplest expressions for $\overline{\mathbf{C}}$ and $\overline{\boldsymbol{\alpha}}$ obtained from (7) or (8) follow from assuming uniform strain $\boldsymbol{\varepsilon}(\mathbf{x}) = \overline{\boldsymbol{\varepsilon}}$ or uniform stress $\boldsymbol{\sigma}(\mathbf{x}) = \overline{\boldsymbol{\sigma}}$ in the aggregate, respectively. In the former case (known as Voigt assumption in elasticity) and if (7) has to be valid for an arbitrary strain and an arbitrary temperature increment, the overall moduli are given by

$$\overline{\mathbf{C}}^{\text{UB}} = \langle \mathbf{C}^{(g)} \rangle \quad \text{and} \quad \overline{\boldsymbol{\alpha}}^{\text{UB}} = \overline{\mathbf{C}}^{UB^{-1}} : \langle \mathbf{C}^{(g)} : \boldsymbol{\alpha}^{(g)} \rangle. \tag{9}$$

Conversely, if the stress is assumed to be uniform in the aggregate (Reuss assumption in elasticity) and (8) holds for an arbitrary stress and an arbitrary temperature increment, the overall moduli are given by the average of the crystal compliances and thermal tensors:

$$\overline{\mathbf{C}}^{\text{LB}} = \langle \mathbf{C}^{(g)^{-1}} \rangle^{-1} \quad \text{and} \quad \overline{\boldsymbol{\alpha}}^{\text{LB}} = \langle \boldsymbol{\alpha}^{(g)} \rangle. \tag{10}$$

The uniform strain approach fulfills compatibility (but not necessarily equilibrium) within the polycrystal and represents an upper bound for the elastic energy of the aggregate. The uniform stress approach fulfills equilibrium (but not necessarily compatibility) in the aggregate and represents a lower bound for the energy. Neither approach fulfills the two conditions given by (7) and (8) simultaneously. In addition, the elastic constants and thermal expansion coefficients given by (9) and (10) are different because the average of the inverses does not coincide with the inverse of the average. Only for the trivial case of elastically and thermally isotropic crystals

are the tensors independent of grain orientation and both averaging procedures give the same results.

The estimation of the effective elastic stiffness $\overline{\mathbf{C}}$ and the effective thermal expansion $\overline{\boldsymbol{\alpha}}$ by means of the SC approach is described in Section 2.5. For this purpose, we first solve the problem of an elastic inclusion embedded in a homogeneous medium. Invoking Mura's [12] concept of equivalent inclusion, the constitutive behavior at the grain level can be rewritten in terms of the homogeneous macroscopic moduli by adding and subtracting $\overline{\mathbf{C}} : \boldsymbol{\varepsilon}(\mathbf{x}) - \overline{\mathbf{C}} : \overline{\boldsymbol{\alpha}} \delta T$ to (3) to obtain

$$\boldsymbol{\sigma}(\mathbf{x}) = \overline{\mathbf{C}} : (\boldsymbol{\varepsilon}(\mathbf{x}) - \boldsymbol{\varepsilon}^*(\mathbf{x})) - \overline{\mathbf{C}} : \overline{\boldsymbol{\alpha}} \delta T, \tag{11}$$

where

$$\boldsymbol{\varepsilon}^*(\mathbf{x}) = \overline{\mathbf{C}}^{-1} : [(\mathbf{C}^{(g)} - \overline{\mathbf{C}}) : \boldsymbol{\varepsilon}(\mathbf{x}) - (\mathbf{C}^{(g)} : \boldsymbol{\alpha}^{(g)} - \overline{\mathbf{C}} : \overline{\boldsymbol{\alpha}}) \delta T]. \tag{12}$$

In this way, the inhomogeneous inclusion is replaced by an equivalent homogeneous inclusion with elastic stiffness $\overline{\mathbf{C}}$ and eigenstrain field $\boldsymbol{\varepsilon}^*(\mathbf{x})$. Subtracting (5) from (11) gives

$$\tilde{\boldsymbol{\sigma}}(\mathbf{x}) = \overline{\mathbf{C}} : (\tilde{\boldsymbol{\varepsilon}}(\mathbf{x}) - \boldsymbol{\varepsilon}^*(\mathbf{x})), \tag{13}$$

where the symbol "˜" denotes local deviations of the corresponding tensor from macroscopic values: $\tilde{\boldsymbol{\sigma}}(\mathbf{x}) = \boldsymbol{\sigma}(\mathbf{x}) - \overline{\boldsymbol{\sigma}}$ and $\tilde{\boldsymbol{\varepsilon}}(\mathbf{x}) = \boldsymbol{\varepsilon}(\mathbf{x}) - \overline{\boldsymbol{\varepsilon}}$.

In the absence of external body forces, the equilibrium equation is

$$\sigma_{ij,j}(\mathbf{x}) = (\overline{\sigma}_{ij} + \tilde{\sigma}_{ij}(\mathbf{x}))_{,j} = \tilde{\sigma}_{ij,j}(\mathbf{x}) = 0. \tag{14}$$

Replacing (13) in (14), using the relation $\tilde{\varepsilon}_{ij}(\mathbf{x}) = (1/2)(\tilde{u}_{i,j}(\mathbf{x}) + \tilde{u}_{j,i}(\mathbf{x}))$, and accounting for the symmetry $\overline{C}_{ijkl} = \overline{C}_{ijlk}$, we get a set of partial differential equations for the local deviation of the displacement gradient field:

$$\overline{C}_{ijkl} \tilde{u}_{k,lj}(\mathbf{x}) + f_i^{\text{ext}}(\mathbf{x}) = 0, \tag{15}$$

where the artificial body force field associated with the heterogeneity of elastic and thermal constants is defined as

$$f_i^{\text{ext}}(\mathbf{x}) = -\overline{C}_{ijkl} \varepsilon_{kl,j}^*(\mathbf{x}) = \sigma_{ij,j}^*(\mathbf{x}). \tag{16}$$

The field $\boldsymbol{\sigma}^*(\mathbf{x}) = -\overline{\mathbf{C}} : \boldsymbol{\varepsilon}^*(\mathbf{x})$ is an eigenstress field, which is also known as polarization field.

2.2. *Green function method*

The system defined by (15) consists of three differential equations with three unknowns, namely, the components of the local deviation of the displacement vector field $\tilde{u}_i(\mathbf{x})$. A system of N linear differential equations with N unknown functions and an inhomogeneity term, such as (15), can be solved using the Green function method. Let us call $G_{km}(\mathbf{x} - \mathbf{x}')$ the Green function associated with $u_i(\mathbf{x})$ of a homogeneous infinite medium with elastic stiffness $\overline{\mathbf{C}}$ that gives, in the absence of any other sources of strain, the displacement at position $\mathbf{x}$ along direction k induced by a unit external body force, with a single non-vanishing component m, applied at $\mathbf{x}$:

$$\overline{C}_{ijkl} G_{km,lj}(\mathbf{x} - \mathbf{x}') + \delta_{im} \delta(\mathbf{x} - \mathbf{x}') = 0, \tag{17}$$

where $\delta(\mathbf{x} - \mathbf{x}')$ is the Dirac delta function and δ_{im} is the Kronecker delta function. Once the solution of (17) is obtained, the solution of (15) is given by the convolution integral, that is, a linear superposition of elementary contributions to the displacement field given by the Green function:

$$u_k(\mathbf{x}) = \int_{R^3} G_{km}(\mathbf{x} - \mathbf{x}') f_m^{\text{ext}}(\mathbf{x}') \, d\mathbf{x}'. \tag{18}$$

Assuming zero macroscopic strain, the same expression holds for $\tilde{u}_i(\mathbf{x})$:

$$\tilde{u}_k(\mathbf{x}) = \int_{R^3} G_{km}(\mathbf{x} - \mathbf{x}') f_m^{\text{ext}}(\mathbf{x}') \, d\mathbf{x}'. \tag{19}$$

Taking the Fourier transform of (17),

$$\overline{C}_{ijkl}FT[G_{km,lj}(\mathbf{x}-\mathbf{x}')] + \delta_{im}FT[\delta(\mathbf{x}-\mathbf{x}')] = 0, \tag{20}$$

and applying the properties of the Fourier transform of the derivative and of the Dirac delta function,

$$\overline{C}_{ijkl}\mathrm{i}^2 k_l k_j \hat{G}_{km}(\mathbf{k}) + \delta_{im} = 0 \tag{21}$$

where $\mathbf{k}$ is a point/vector of the 3D Fourier space of angular frequencies and $\mathrm{i} = \sqrt{-1}$ is the imaginary unit. Denoting $\mathbf{k} = k\boldsymbol{\alpha}$, where the scalar k and the vector $\boldsymbol{\alpha}$ (this notation is only used here and in the next section, and it should not be confused with the thermal expansion tensors α_{ij} used elsewhere) are the modulus and the unit vector associated with $\mathbf{k}$, respectively, we obtain

$$\overline{C}_{ijkl}\alpha_l \alpha_j [k^2 \hat{G}_{km}(\mathbf{k})] = \delta_{im}. \tag{22}$$

Defining

$$A_{ik}(\boldsymbol{\alpha}) = \alpha_j \alpha_l \overline{C}_{ijkl} \tag{23}$$

allows us to obtain the algorithmic expression to calculate the Fourier transform of the Green function:

$$k^2 \hat{G}_{ij}(\boldsymbol{\alpha}) = A_{ij}^{-1}(\boldsymbol{\alpha}). \tag{24}$$

Since the matrix A_{ij} is a real function of $\boldsymbol{\alpha}$, so is $k^2 \hat{G}_{ij}$. This property leads to real integrals in the derivation that follows.

2.3. *Elastic inclusion and Eshelby tensor*

Replacing the eigenstress given by (16) in (19) and taking derivatives yield for the local deviation of the displacement gradient field

$$\tilde{u}_{k,l}(\mathbf{x}) = \int_{R^3} G_{ki,l}(\mathbf{x}-\mathbf{x}')\sigma_{ij,j}^*(\mathbf{x}')\,\mathrm{d}\mathbf{x}'. \tag{25}$$

Using the relation $\partial G_{ij}(\mathbf{x}-\mathbf{x}')/\partial\mathbf{x} = -\partial G_{ij}(\mathbf{x}-\mathbf{x}')/\partial\mathbf{x}'$, we can rewrite the integrand of (25) as $G_{ki,l}(\mathbf{x}-\mathbf{x}')\sigma_{ij,j}^*(\mathbf{x}') = (G_{ki,l}(\mathbf{x}-\mathbf{x}')\sigma_{ij}^*(\mathbf{x}'))_{,j} + G_{ki,lj}(\mathbf{x}-\mathbf{x}')\sigma_{ij}^*(\mathbf{x}')$ for integration by parts. Using the Gauss theorem and the vanishing character of the Green function at infinity, we obtain [12]

$$\tilde{u}_{k,l}(\mathbf{x}) = \int_{R^3} G_{ki,jl}(\mathbf{x}-\mathbf{x}')\sigma_{ij}^*(\mathbf{x}')\,\mathrm{d}\mathbf{x}'. \tag{26}$$

Equation (26) provides an exact implicit solution to the problem of a general eigenstrain field $\boldsymbol{\varepsilon}^*(\mathbf{x})$ being accommodated elastically and inducing an eigenstress field $\boldsymbol{\sigma}^*(\mathbf{x})$. Such a solution requires knowing the local dependence of the eigenstrain or the eigenstress tensor. Here, we are interested in the specific application to thermo-elastic aggregates, where the elastic stiffness $\mathbf{C}^{(g)}$, the thermal expansion tensor $\boldsymbol{\alpha}^{(g)}$, and the thermal dilatation $\boldsymbol{\alpha}^{(g)}\delta T$ are constant over the domain of each grain. This leads to the eigenstrain $\boldsymbol{\varepsilon}^{*(g)}$ adopting a constant value in the domain of the inclusion and being zero in the domain of the effective medium. Under these conditions, Eshelby [13] and Mura [12] demonstrated that for a single inclusion of ellipsoidal shape embedded in an infinite medium, the elastic strain field is uniform in the domain of the inclusion. Here, however, we follow the more general approach of Berveiller *et al.* [14], expressing the average of the local deviation of the displacement gradient field given by (25) over the domain Ω^g of the grain:

$$\tilde{u}_{k,l}^{(g)} = \left(-\frac{1}{\Omega^g}\int_{\Omega^g}\int_{\Omega^g} G_{ki,jl}(\mathbf{x}-\mathbf{x}')\,\mathrm{d}\mathbf{x}\,\mathrm{d}\mathbf{x}'\right)\overline{C}_{ijmn}\varepsilon_{mn}^{*(g)}. \tag{27}$$

Equation (27) can be interpreted in two ways. If the effective elastic modulus $\overline{\mathbf{C}}$ is assumed to be the stiffness of an infinite homogeneous matrix in which an ellipsoidal inclusion with constant eigenstrain $\boldsymbol{\varepsilon}^{*(g)}$ is embedded, $\tilde{u}_{k,l}^{(g)}$ is the constant value inside domain Ω^g obtained from the

solution of Eshelby's inclusion problem. On the other hand, in the actual case of a polycrystal, $\tilde{u}_{k,l}^{(g)}$ should be interpreted as the average value (first moment) of the corresponding field in grain (g).

Expressing the second derivative of the Green tensor in terms of its Fourier transform, we obtain

$$\tilde{u}_{k,l}^{(g)} = \left(\frac{1}{8\pi^3 \Omega^g} \int_{\Omega^g} \int_{\Omega^g} \int_{K^3} (\alpha_l \alpha_j k^2 \hat{G}_{ki}(\mathbf{k})) \exp[-i\mathbf{k}\cdot(\mathbf{x}-\mathbf{x}')] \, d\mathbf{k}\, d\mathbf{x}\, d\mathbf{x}' \right) \overline{C}_{ijmn} \varepsilon_{mn}^{*(g)}$$
$$= T_{klij} \overline{C}_{ijmn} \varepsilon_{mn}^{*(g)}. \tag{28}$$

Transforming the integral over the reciprocal space to spherical coordinates such that $d\mathbf{k} = \sin\theta\, d\theta\, d\phi\, k^2\, dk$ and using (22), the tensor T_{klij} can be rewritten as

$$T_{klij} = \frac{1}{8\pi^3 \Omega^g} \int_0^{2\pi} \int_0^{\pi} \alpha_l \alpha_j A_{ki}^{-1}(\boldsymbol{\alpha}) \Lambda(\boldsymbol{\alpha}) \sin\theta\, d\theta\, d\varphi, \tag{29}$$

where θ and ϕ are the spherical coordinates of the Fourier unit vector $\boldsymbol{\alpha}$ and

$$\Lambda(\boldsymbol{\alpha}) = \int_0^{\infty} \left(\int_{\Omega^g} \int_{\Omega^g} \exp[-ik(\mathbf{x}-\mathbf{x}')] \, d\mathbf{x}\, d\mathbf{x}' \right) k^2\, dk. \tag{30}$$

Integration of (30) inside an ellipsoidal domain Ω^g with main axes (a,b,c) gives [14]

$$\Lambda(\boldsymbol{\alpha}) = \frac{8\pi^3}{3} \frac{(abc)^2}{[\rho(\boldsymbol{\alpha})]^3}, \tag{31}$$

where

$$\rho(\boldsymbol{\alpha}) = \sqrt{(a\alpha_1)^2 + (b\alpha_2)^2 + (c\alpha_3)^2}. \tag{32}$$

Replacing (31) in (29), and recalling that $\Omega^g = (4/3)\pi(abc)$, provides an expression of T_{klij} for an ellipsoidal grain:

$$T_{klij} = \frac{(abc)}{4\pi} \int_0^{2\pi} \int_0^{\pi} \frac{\alpha_j \alpha_l A_{ki}^{-1}(\boldsymbol{\alpha})}{[\rho(\boldsymbol{\alpha})]^3} \sin\theta\, d\theta\, d\varphi. \tag{33}$$

For arbitrary elastic anisotropy, the double integral in (33) has to be solved numerically using, for instance, a Gauss–Legendre technique [5]. For the purpose of calculating the symmetric strain tensor, the following symmetric Eshelby tensor is defined:

$$S_{ijkl} = \tfrac{1}{4}(T_{ijmn} + T_{jimn} + T_{ijnm} + T_{jinm})\overline{C}_{mnkl}. \tag{34}$$

2.4. Interaction and localization equations

Taking the symmetric part of (28), and using the Eshelby tensor defined in (34), we obtain the average deviation of strain in grain (g) with respect to the macroscopic strain:

$$\tilde{\boldsymbol{\varepsilon}}^{(g)} = \mathbf{S} : \boldsymbol{\varepsilon}^{*(g)}. \tag{35}$$

An expression equivalent to (13), relating local deviations in stress, strain, and eigenstrain fields, also holds for the deviations of average stress, average strain, and average eigenstrain in the grains with respect to the effective medium. It is straightforward to demonstrate this by integrating (13) over the grain domain:

$$\tilde{\boldsymbol{\sigma}}^{(g)} = \overline{\mathbf{C}} : (\tilde{\boldsymbol{\varepsilon}}^{(g)} - \boldsymbol{\varepsilon}^{*(g)}). \tag{36}$$

Replacing the eigenstrain given by (35) in (36), the following *interaction equation* is obtained:

$$\tilde{\boldsymbol{\sigma}}^{(g)} = -\tilde{\mathbf{C}} : \tilde{\boldsymbol{\varepsilon}}^{(g)}, \tag{37}$$

where the *interaction tensor* is defined as

$$\tilde{\mathbf{C}} = \overline{\mathbf{C}} : (\mathbf{I} - \mathbf{S}) : \mathbf{S}^{-1}. \tag{38}$$

Using the polycrystal constitutive relation (5) and the grain-averaged constitutive relation obtained from averaging (3) in the domain of grain (g),

$$\boldsymbol{\sigma}^{(g)} = \mathbf{C}^{(g)} : \boldsymbol{\varepsilon}^{(g)} - \mathbf{C}^{(g)} : \boldsymbol{\alpha}^{(g)} \delta T, \tag{39}$$

the interaction equation (37) can be rewritten in terms of total strain tensors. After some algebraic manipulation, the following *strain localization equation* is obtained:

$$\boldsymbol{\varepsilon}^{(g)} = \mathbf{A}^{(g)} : \overline{\boldsymbol{\varepsilon}} + \mathbf{D}^{(g)} \delta T, \tag{40}$$

where the strain localization tensors are defined as

$$\mathbf{A}^{(g)} = (\mathbf{C}^{(g)} + \tilde{\mathbf{C}})^{-1} : (\overline{\mathbf{C}} + \tilde{\mathbf{C}}), \tag{41}$$

$$\mathbf{D}^{(g)} = (\mathbf{C}^{(g)} + \tilde{\mathbf{C}})^{-1} : (\mathbf{C}^{(g)} : \boldsymbol{\alpha}^{(g)} - \overline{\mathbf{C}} : \overline{\boldsymbol{\alpha}}). \tag{42}$$

2.5. *Self-consistent equations*

The derivation presented in the previous sections solves the problem of a thermo-elastic inclusion embedded in a thermo-elastic effective medium being subject to external loading conditions. In this section, we use the previous result to construct a polycrystal model, consisting in regarding each grain as an ellipsoidal inclusion embedded in a homogeneous medium with the same properties as those of the homogenized polycrystal. The properties of such a medium are not known *a priori*, and they will be obtained following an iterative SC procedure. The corresponding equations are derived in this section.

The homogenized medium assumption is central to our derivation and needs some discussion. Even if the solution for each individual ellipsoid representing a grain embedded in a homogeneous medium is exact, in a real aggregate, grains are not ellipsoidal and are not surrounded by a homogeneous continuum. Rather, the surrounding neighbors have different orientations and induce stress gradients inside the grains and across grain boundaries. In addition, grains with the same orientation in the aggregate are surrounded by different neighbors, and as a consequence, their associated average stress is not the same. As a result, the grain stress and strain given by the effective medium approximation have to be regarded as representing the average state of all grains having the same orientation in the aggregate.

We use the localization equation for the strain (40) to derive two equations. The first equation follows from replacing (40) in (39):

$$\boldsymbol{\sigma}^{(g)} = \mathbf{C}^{(g)} : \boldsymbol{\varepsilon}^{(g)} - \mathbf{C}^{(g)} : \boldsymbol{\alpha}^{(g)} \delta T = \mathbf{C}^{(g)} : \mathbf{A}^{(g)} : \overline{\boldsymbol{\varepsilon}} + (\mathbf{C}^{(g)} : \mathbf{D}^{(g)} - \mathbf{C}^{(g)} : \boldsymbol{\alpha}^{(g)}) \delta T. \tag{43}$$

The second equation follows from taking the average of (40) over all grains:

$$\langle \boldsymbol{\varepsilon}^{(g)} \rangle = \langle \mathbf{A}^{(g)} \rangle : \overline{\boldsymbol{\varepsilon}} + \langle \mathbf{D}^{(g)} \rangle \delta T. \tag{44}$$

We recall that $\langle \ \rangle$ denotes the average over the representative grains weighted by the associated grain volume fraction. Extracting the effective strain of the medium $\overline{\boldsymbol{\varepsilon}} = \langle \boldsymbol{\varepsilon}^{(g)} \rangle$ from (44), replacing it in (43), and averaging the grain stresses give

$$\langle \boldsymbol{\sigma}^{(g)} \rangle = \langle \mathbf{C}^{(g)} : \mathbf{A}^{(g)} \rangle : (\langle \mathbf{A}^{(g)} \rangle^{-1} : \langle \boldsymbol{\varepsilon}^{(g)} \rangle - \langle \mathbf{A}^{(g)} \rangle^{-1} : \langle \mathbf{D}^{(g)} \rangle \delta T)$$
$$+ \langle \mathbf{C}^{(g)} \mathbf{D}^{(g)} - \mathbf{C}^{(g)} : \boldsymbol{\alpha}^{(g)} \rangle \delta T. \tag{45}$$

Enforcing the condition that the effective stress is equal to the average of the grain stresses $\overline{\boldsymbol{\sigma}} = \langle \boldsymbol{\sigma}^{(g)} \rangle$,

$$\overline{\boldsymbol{\sigma}} = \overline{\mathbf{C}} : \overline{\boldsymbol{\varepsilon}} - \overline{\mathbf{C}} : \overline{\boldsymbol{\alpha}} \delta T = \langle \boldsymbol{\sigma}^{(g)} \rangle, \tag{46}$$

leads to

$$\overline{\mathbf{C}} : \overline{\boldsymbol{\varepsilon}} - \overline{\mathbf{C}} : \overline{\boldsymbol{\alpha}} \delta T = \langle \mathbf{C}^{(g)} : \mathbf{A}^{(g)} \rangle : \langle \mathbf{A}^{(g)} \rangle^{-1} : \overline{\boldsymbol{\varepsilon}}$$
$$- \{ \langle \mathbf{C}^{(g)} : \mathbf{A}^{(g)} \rangle : \langle \mathbf{A}^{(g)} \rangle^{-1} : \langle \mathbf{D}^{(g)} \rangle - \mathbf{C}^{(g)} : \mathbf{D}^{(g)} + \mathbf{C}^{(g)} : \boldsymbol{\alpha}^{(g)} \} \delta T. \tag{47}$$

For this identity to hold, the strain and temperature factors on the right-hand side have to coincide with those on the left-hand side. This condition leads to

$$\overline{\mathbf{C}} = \langle \mathbf{C}^{(g)} : \mathbf{A}^{(g)} \rangle : \langle \mathbf{A}^{(g)} \rangle^{-1}, \tag{48}$$

which is an implicit equation for the stiffness because the localization tensor $\mathbf{A}^{(g)}$ is a function of the interaction tensor $\tilde{\mathbf{C}}^{(g)}$ (38), which in turn is a function of $\overline{\mathbf{C}}$ and the Eshelby tensor $\mathbf{S}$, which is also a function of $\overline{\mathbf{C}}$. As a consequence, Equation (48) is a fixed-point equation for the effective polycrystal's elastic stiffness.

The condition on the term associated with a temperature change is

$$\overline{\mathbf{C}} : \overline{\boldsymbol{\alpha}} = \langle \mathbf{A}^{\dagger(g)} : \mathbf{D}^{(g)} \rangle + \langle \mathbf{C}^{(g)} : \boldsymbol{\alpha}^{(g)} \rangle, \tag{49}$$

where

$$\mathbf{A}^{\dagger(g)} = (\overline{\mathbf{C}} + \tilde{\mathbf{C}}^{(g)}) : (\mathbf{C}^{(g)} + \tilde{\mathbf{C}}^{(g)})^{-1}. \tag{50}$$

Using (42) for $\mathbf{D}^{(g)}$ leads, after some algebraic manipulation, to a direct equation giving the effective thermal coefficients of the aggregate:

$$\overline{\mathbf{C}} : \overline{\boldsymbol{\alpha}} = \langle \mathbf{A}^{\dagger(g)} \rangle^{-1} : \langle \mathbf{A}^{\dagger(g)} : \mathbf{C}^{(g)} : \boldsymbol{\alpha}^{(g)} \rangle. \tag{51}$$

The iterative solution of (48) gives the polycrystal's elastic stiffness, and the subsequent use of (51) gives the polycrystal's thermal coefficients once the effective stiffness is known.

We end this section mentioning that by taking derivatives with respect to the local moduli of the effective properties given by (48) and (51), it is possible to access information on intragranular heterogeneity in the form of second moments of the stress field distribution in each mechanical phase (g). The algorithms to calculate these second moments from the SC theory for thermoelastic polycrystals (based on the original TESC expressions for composites [15, 16]) can be found in [17–19].

3. Applications

The applications discussed in this section include the calculation of effective elastic and thermal moduli of zirconium, beryllium, and uranium and the evolution of macroscopic strain and internal stresses during cooling processes.

3.1. *Cooling of zirconium*

The purpose of this example is to show how texture affects the effective elastic and thermal constants and also the evolution of internal stress during cooling. We simulate cooling of Zr from 900 to 300 K for two different crystal orientation distributions: a non-textured aggregate (see discussion in the next paragraph) and an aggregate with axisymmetric texture, typical of an extruded bar. The axisymmetric texture is displayed in Figure 1, and the single-crystal elastic and thermal constants (or coefficients of thermal expansion) are given in Tables 1 [20] and 2 [21], respectively. In this simulation, the boundary condition is that the macroscopic stress components are zero, and at 900 K, the grains in the aggregate are assumed to be stress-free.

The UB, LB, and TESC elastic constants calculated using 1000 orientations from a Sobol sequence [22], obtained by maximizing the separation (in Euler space) of the next orientation in the sequence from all the previous orientations, are given in Table 1. The effective thermal moduli are given in Table 2. Observe that the effective properties may deviate slightly from the exact isotropic conditions ($\overline{C}_{11} = \overline{C}_{22} = \overline{C}_{33}$ and $\overline{\alpha}_1 = \overline{\alpha}_2 = \overline{\alpha}_3$); for example, note some small fluctuations in the least significant digits in the predicted values for non-textured aggregates. The reason is that despite the aforementioned Sobol sequence optimizing the generation of a

Table 1. Zr single-crystal elastic constants [20] and polycrystal elastic constants predicted using UB, LB, and TESC models for non-textured and extrusion-texture aggregates (Voigt notation; units of [GPa])

	C_{11}	C_{22}	C_{33}	C_{23}	C_{13}	C_{12}	C_{44}	C_{55}	C_{66}
Crystal	143.5	143.5	164.9	65.4	65.4	72.5	32.1	32.1	35.5
				Non-textured aggregate					
UB	144.1	144.1	144.1	71.1	71.0	71.1	36.5	36.5	36.5
TESC	143.5	143.5	143.5	71.2	71.2	71.2	36.1	36.1	36.1
LB	142.9	142.9	142.9	71.4	71.4	71.4	35.8	35.8	35.8
				Textured aggregate					
UB	146.9	146.5	142.4	70.0	69.9	71.3	35.0	34.9	37.8
TESC	145.9	145.7	142.2	70.2	70.1	71.6	34.8	34.7	37.2
LB	145.1	144.8	142.0	70.4	70.3	71.9	34.6	34.6	36.7

Table 2. Zr single-crystal thermal constants [21] and polycrystal thermal constants predicted using UB, LB, and TESC models for non-textured and extrusion-texture aggregates (Voigt notation; units of [10^{-6} K^{-1}])

	α_1	α_2	α_3	α_1	α_2	α_3
Crystal	5.7	5.7	10.5	5.7	5.7	10.5
		Non-textured			Textured	
UB	7.28	7.29	7.28	8.09	8.02	5.71
TESC	7.23	7.23	7.23	7.98	7.91	5.87
LB	7.23	7.23	7.23	7.87	7.82	6.00

discrete set of orientations to a uniform distribution, which should produce the same effective response as that for a very large set of random orientations, the set of 1000 orientations used here for representing the aggregate is not strictly uniform. In what follows, the polycrystal represented by these 1000 orientations is referred to as "non-textured aggregate."

Since Zr is mildly anisotropic elastically, the stiffness components of the textured aggregate are not very different from those of the non-textured aggregate, but they display a clear axial symmetry, that is, $C_{11} \cong C_{22} \neq C_{33}$, $C_{13} \cong C_{23} \neq C_{12}$, and $C_{44} \cong C_{55} \neq C_{66}$. On the other hand, the large thermal anisotropy of the single-crystal thermal coefficients makes the effective properties strongly dependent on texture. As we show next, it also has an important effect on the internal stress evolution during cooling.

Figure 2 displays the evolution of overall diagonal strain components as a function of decreasing temperature predicted using TESC. As is to be expected, for the non-textured aggregate, all three directions contract by the same amount; but for the textured aggregate, this is not the case. A concentration of basal poles perpendicular to the axial direction of the bar, combined with a larger thermal coefficient along the c-axis, leads to a larger contraction perpendicular to the bar axis. This is consistent with the effective thermal coefficients of the aggregate reported in Table 2.

Figure 2 also shows the evolution with temperature of the strain normal to basal (0002) and prismatic (10–10) planes either perpendicular to axis 1 (radial direction) or axis 3 (axial direction) of the texture. In the case of the non-textured aggregate, both directions are equivalent, and the result reflects the fact that the tendency of the crystal is to contract more than the effective medium along the c-axis and less than the effective medium along the a-axis. The interaction of the grain (inclusion) with the effective medium partially prevents such behavior, and this leaves
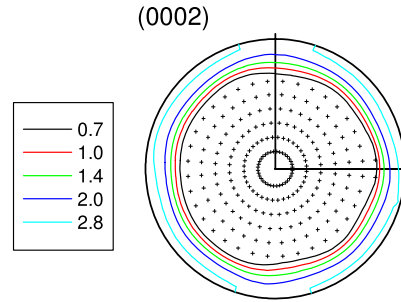
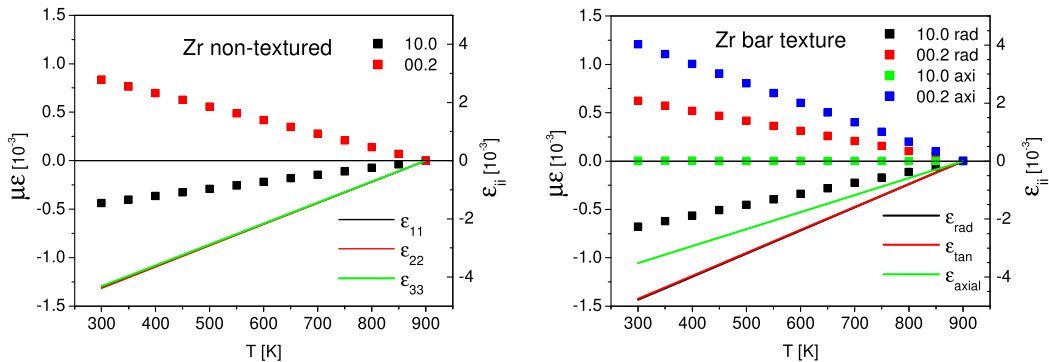**Figure 1.** Basal pole figure of extruded Zr bar.

Figure 2. Microstrain evolution in (10–10) and (0002) planes and macroscopic strain evolution with temperature in non-textured Zr and extruded Zr bar when cooling from 900 K to 300 K, predicted using TESC.

the *c*-axis in tension and the *a*-axis in compression. The same mechanism applies to internal stress evolution in the textured polycrystal except that now the average contraction is different along the axial and radial directions and so is the interaction with grains oriented in either of these directions. The TESC model captures well such a directional interaction. Observe that the final elastic strains are large ($\sim 1 \times 10^{-3}$) and correspond to normal stresses of order 100 MPa. The larger thermal coefficient perpendicular to the basal plane induces a larger thermal contraction, which is counteracted by the interaction with the surrounding medium. As a consequence, the strain along the *c*-axis is always positive. The opposite is true for the direction normal to the prismatic planes of the crystal. Texture changes the properties of the effective medium and affects the result quantitatively. These predictions are consistent with measurements in a Zrly-2 bar reported by MacEwen *et al.* [21].

3.2. *Cooling of beryllium*

To show the relevance of the single-crystal anisotropic moduli, here we perform the same calculations for another hcp material, beryllium, and compare the results against those for zirconium. For this purpose, we simulate cooling of Be from 900 to 300 K for a non-textured aggregate. The single-crystal elastic and thermal constants are given in Tables 3 [20] and 4 [23], respectively. As before, the boundary condition is zero macroscopic stress components and an internal stress-free aggregate at 900 K. The latter is in reasonable agreement with the internal stresses measured by Brown *et al.* [24] as a function of temperature in a non-textured aggregate.

Table 3. Be single-crystal elastic constants [20] and polycrystal elastic constants predicted using UB, LB, and TESC models for a non-textured aggregate (Voigt notation; units of [GPa])

	C_{11}	C_{22}	C_{33}	C_{23}	C_{13}	C_{12}	C_{44}	C_{55}	C_{66}
Crystal	292.3	292.3	336.4	14.0	14.0	26.7	162.5	162.5	132.8
			Non-textured aggregate						
UB	313.6	313.6	313.6	14.9	15.9	14.9	149.3	149.3	149.3
TESC	312.5	312.6	312.5	15.3	15.3	15.3	148.6	148.6	148.6
LB	311.5	311.3	311.5	15.6	15.6	15.6	148.0	148.0	148.0

Table 4. Be single-crystal thermal constants at 450 K [23] and polycrystal thermal constants predicted using UB, LB, and TESC models for a non-textured aggregate (Voigt notation; units of $[10^{-6} \text{ K}^{-1}]$)

	α_1	α_2	α_3
Crystal	13.9	13.9	10.4
		Non-textured	
UB	12.7	12.7	12.7
TESC	12.7	12.7	12.7
LB	12.7	12.7	12.7

Beryllium is a peculiar hcp material in two aspects: it exhibits an unusually low Poisson modulus ($v \sim 0.045$; varies depending on the crystal direction) and its thermal expansion coefficients have been reported to increase two-fold from 300 to 900 K [23]. For the purpose of this demonstration, we have made no attempt at accounting for the variation in thermal coefficients with temperature and have adopted the coefficients corresponding to 450 K. Another difference from Zr is that thermal contraction along the c-axis is smaller than perpendicular to it since $\alpha_{33} < \alpha_{11}$.

The UB, LB, and TESC polycrystal elastic constants are given in Table 3 and the corresponding polycrystal thermal moduli are given in Table 4.

Figure 3 displays the evolution of overall diagonal strain components as a function of decreasing temperature predicted using TESC. As is to be expected for a non-textured aggregate, all three directions contract by the same amount, about 0.8% at room temperature. Figure 3 also shows the evolution with temperature of the strain normal to basal (0002) and prismatic (10–10) planes, and the result reflects the tendency of the crystal to contract less than the effective medium along the c-axis and more than the effective medium along the a-axis. The interaction of the grain (inclusion) with the effective medium opposes such a trend, and this leaves the c-axis in compression and the a-axis in tension, which is opposite to what happens in Zr. The TESC model captures such a directional interaction and predicts the final crystallographic elastic strains of $\sim 0.5 \times 10^{-3}$, which correspond to large normal stresses of order ~ 100 MPa in prism planes and of ~ -200 MPa in basal planes (Figure 3). These values are in good agreement with the measurements reported by Brown *et al.* [24]. Although the internal stresses are somewhat smaller in a textured aggregate, they are expected to play an important role in early yielding, stress differential, and elastoplastic transition when a Be aggregate is subjected to mechanical loading.

3.3. *Cooling of uranium*

As in the previous cases, the purpose of this example is to show how texture affects the effective elastic and thermal constants, and the evolution of internal stress, during cooling of α-U. In α-U,
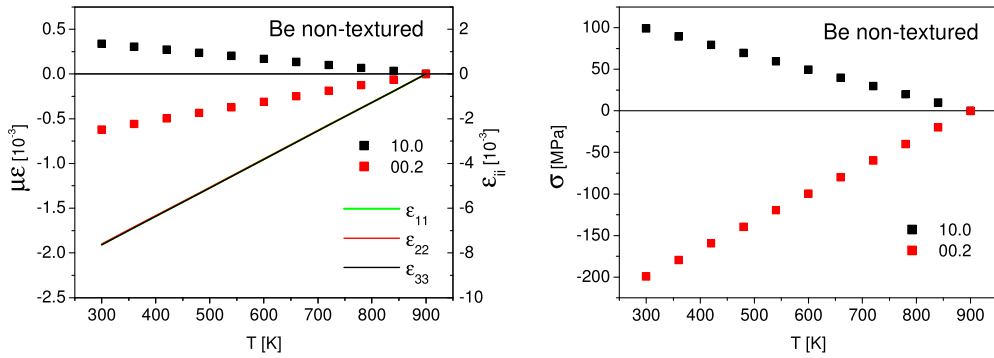
Figure 3. Microstrain evolution in (10–10) and (0002) planes and macroscopic strain evolution with temperature predicted using TESC for non-textured Be when cooling from 900 to 300 K (left); evolution of stress normal to (10–10) and (0002) planes (right).
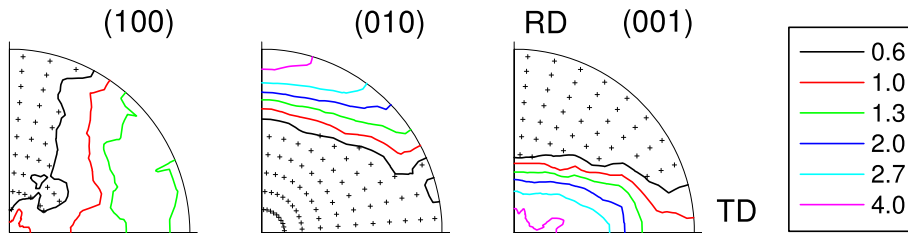

Figure 4. (100), (010), and (001) poles of rolled α-uranium.

the elastic and thermal constants are more anisotropic than those of Zr, and the single-crystal symmetry is orthotropic instead of hexagonal.

As before, to evidence texture effects, we simulate the cooling of α-U from 900 to 300 K for two different crystal orientation distributions: a non-textured aggregate and an aggregate with rolling texture, see Figure 4. The single-crystal elastic and thermal coefficients are reported in Tables 5 and 6, respectively. The evolution of internal strains on {100}, {010}, and {001} planes along directions x_1 (rolling), x_2 (transverse), and x_3 (normal) is also reported. The simulation imposes all the macroscopic stress components to be zero while cooling from 900 to 300 K.

The UB, LB, and TESC elastic constants calculated for the non-textured and textured aggregates are given in Table 5 and the effective thermal moduli are given in Table 6. The large anisotropy of the α-U single-crystal thermal coefficients makes the effective properties strongly dependent on texture. In addition, as shown in Figure 5 (and also in Figure 2 for Zr), the macroscopic strains induced by cooling under the condition of zero macroscopic stress are contractive. The grains, however, develop increasingly compressive and tensile components of stress and elastic strain that average to zero.

The larger thermal coefficients along the [100] and [001] crystal directions, compared with [010], induce a larger thermal contraction perpendicular to those planes, which is counteracted by the interaction with the surrounding medium. As a consequence, the associated internal strains are always positive. The opposite is true for the [010] crystal direction, which has a nearly zero thermal coefficient. Texture changes the properties of the effective medium and affects the results quantitatively but not qualitatively.
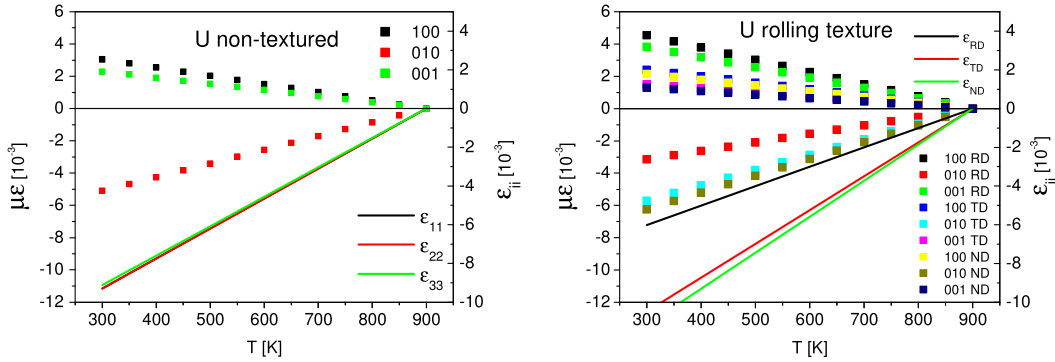
Figure 5. Evolution of microstrains in {100}, {010}, and {001} planes and evolution of macroscopic strain components in non-textured and rolling-texture α-U when cooling from 900 to 300 K.

Table 5. α-uranium single-crystal elastic constants [25] and polycrystal elastic constants predicted using UB, LB, and TESC models for a non-textured and a rolling-texture aggregate (Voigt notation; units of [GPa])

	C_{11}	C_{22}	C_{33}	C_{23}	C_{13}	C_{12}	C_{44}	C_{55}	C_{66}
Crystal	214.8	198.6	267.1	107.6	21.8	46.5	124.4	73.4	74.3
				Non-textured aggregate					
UB	232.2	232.3	232.1	55.9	56.1	55.9	88.0	88.1	87.9
SC	225.1	225.2	225.1	56.7	56.7	56.6	84.1	84.2	84.1
LB	219.0	219.1	219.0	57.6	57.7	57.5	80.6	80.7	80.6
				Textured aggregate					
UB	214.0	224.3	241.3	52.3	65.4	58.6	92.3	94.5	85.8
SC	208.5	219.0	233.7	52.8	65.7	59.2	88.7	90.2	81.9
LB	203.8	214.5	227.0	53.5	66.1	59.9	85.5	86.3	78.5

Table 6. α-uranium single-crystal thermal constants [26]. Polycrystal thermal constants predicted using UB, LB, and TESC models for a non-textured and a rolling-texture aggregate (Voigt notation; units of [10^{-6} K^{-1}])

	α_1	α_2	α_3	α_1	α_2	α_3
Single crystal	25.41	0.65	20.65	25.41	0.65	20.65
	Non-textured			Textured		
UB	15.11	15.15	15.11	10.64	17.17	17.44
SC	15.38	15.41	15.37	10.01	17.46	18.61
LB	15.56	15.60	15.55	9.21	17.64	19.86

4. Conclusions

In this paper, the TESC formulation is presented in detail and applied to the cooling of polycrystalline single-phase non-cubic metals. The TESC model captures the effect of crystallographic texture and single-crystal elastic and thermal anisotropy on effective and local thermo-elastic responses.

Although not shown here, the TESC model can be applied to multiphase polycrystalline aggregates. In such cases, the heterogeneity in the local thermal response captured by the model arises from single-crystal thermal anisotropy (i.e. for non-cubic phases) and/or the difference in thermal properties between phases (including cubic phases).

The results presented here show that depending on temperature change, texture of the aggregate, and level of single-crystal elastic and thermal anisotropy, internal stresses at the grain level can be significant even in the absence of applied stress, for example, cooling under zero external stresses, as in all the cases presented. These internal stresses may play an important role in promoting plastic yield during cooling or during loading after annealing as well as in determining subsequent stress differential, for example, different yield in tension versus compression. In other words, these thermal stresses can significantly affect yielding and the elastoplastic transition compared with the case of aggregates with stress-free grains. Evidently, the TESC formulation presented here is not able to capture this effect by itself, but it needs to be combined with model extensions that include crystal plasticity mechanisms such as elastoplastic [27] and elastoviscoplastic [28, 29] formulations.

References

[1] A. V. Hershey, "The elasticity of an isotropic aggregate of anisotropic cubic crystals", *J. Appl. Mech.-Trans. ASME* **21** (1954), p. 236.

[2] E. Kröner, "Berechnung der elastischen Konstanten des Vielkristalls aus den Konstanten des Einkristalls", *Z. Phys.* **15** (1958), p. 504.

[3] R. Hill, "Continuum micro-mechanics of elastoplastic polycrystals", *J. Mech. Phys. Solids* **13** (1965), p. 89.

[4] R. Zeller, P. H. Dederichs, "Elastic constants of polycrystals", *Phys. Status Solidi (b)* **55** (1973), p. 831.

[5] C. N. Tomé, R. A. Lebensohn, "ViscoPlastic Self-Consistent (VPSC) code", Los Alamos National Laboratory.

[6] L. J. Walpole, "On the overall elastic moduli of composite materials", *J. Mech. Phys. Solids* **17** (1969), p. 235.

[7] J. R. Willis, "Variational and related methods for the overall properties of composites", *Adv. Appl. Mech.* **21** (1981), p. 1.

[8] V. A. Buryachenko, "Multiparticle effective field and related methods in micromechanics of random structure composites", *Math. Mech. Solids* **6** (2001), p. 577.

[9] G. W. Milton, *The Theory of Composites*, Cambridge University Press, 2002.

[10] C. N. Tomé, N. Christodoulou, P. A. Turner, M. A. Miller, C. H. Woo, J. Root, T. M. Holden, "Role of internal stresses in the transient of irradiation growth of Zircaloy-2", *J. Nucl. Mater.* **227** (1996), p. 237.

[11] R. Hill, "The essential structure of constitutive laws for metal composites and polycrystals", *J. Mech. Phys. Solids* **15** (1967), p. 79.

[12] T. Mura, *Micromechanics of Defects in Solids*, 2nd ed., Martinus-Nijhoff Publishers, Dordrecht, The Netherlands, 1987.

[13] J. D. Eshelby, "The determination of the elastic field of an ellipsoidal inclusion, and related problems", *Proc. R. Soc. Lond. A* **241** (1957), p. 366.

[14] M. Berveiller, O. Fassi-Fehri, A. Hihi, "The problem of two plastic and heterogeneous inclusions in an anisotropic medium", *Int. J. Eng. Sci.* **25** (1987), p. 691.

[15] M. Bobeth, G. Diener, "Static elastic and thermoelastic fluctuations in multiphase composites", *J. Mech. Phys. Solids* **35** (1987), p. 37.

[16] W. Kreher, "Residual stresses and stored elastic energy of composites and polycrystals", *J. Mech. Phys. Solids* **38** (1990), p. 115.

[17] Y. Liu, "Macroscopic behavior, fluctuations and texture evolution in viscoplastic polycrystals", PhD Thesis, University of Pennsylvania, USA, 2003.

[18] R. Brenner, O. Castelnau, L. Badea, "Mechanical field fluctuations in polycrystals estimated by homogenization techniques:", *Proc. R. Soc. Lond. A* **460** (2004), p. 3589.

[19] R. A. Lebensohn, C. N. Tomé, P. P. Castañeda, "Self-consistent modeling of the mechanical behavior of viscoplastic polycrystals incorporating intragranular field fluctuations", *Phil. Mag.* **87** (2007), p. 4287.

[20] G. Simmons, H. Wang, *Single Crystal Elastic Constants and Calculated Aggregate Properties: A Handbook*, MIT Press, 1971.

[21] S. R. MacEwen, C. N. Tomé, J. Faber Jr., "Residual stresses in annealed Zircaloy", *Acta Metall.* **37** (1989), p. 979.

[22] O. Castelnau, D. K. Blackman, R. A. Lebensohn, P. P. Castañeda, "Micromechanical modelling of the viscoplastic behavior of olivine", *J. Geophys. Res. B* **113** (2008), p. B09202.

[23] P. Gordon, "A high temperature precision X-ray camera. Some measurements of the thermal coefficients of expansion of Beryllium", *J. Appl. Phys.* **20** (1949), p. 908.

[24] D. W. Brown, T. A. Sisneros, B. Clausen, S. Abeln, M. A. M. Bourke, B. G. Smith, M. L. Steinzig, C. N. Tomé, S. C. Vogel, "Development of intergranular thermal residual stresses in Beryllium during cooling from processing temperatures", *Acta Mater.* **57** (2009), p. 972.

[25] E. S. Fisher, "Temperature dependence of the elastic moduli in α-uranium single crystals", *J. Nucl. Mater.* **18** (1966), p. 39.

[26] L. T. Lloyd, C. S. Barrett, "Thermal expansion of α-uranium", *J. Nucl. Mater.* **18** (1966), p. 55.

[27] P. A. Turner, C. N. Tomé, "A study of residual stresses in Zircaloy-2 with rod texture", *Acta Metall. Mater.* **42** (1994), p. 4143.

[28] Y. Jeong, C. N. Tomé, "Extension of the visco-plastic self-consistent model to account for elasto-visco-plastic behavior using a perturbed visco-plastic approach", *Modell. Simul. Mater. Sci. Eng.* **27** (2019), article no. 085013.

[29] M. Zecevic, R. A. Lebensohn, "New robust self-consistent homogenization schemes of elasto-viscoplastic polycrystals", *Int. J. Solids Struct.* **202** (2020), p. 434.